Electronic Supporting Information (ESI)

Stabilizing $NiCo_2O_4$ hybrid architectures by reduced graphene oxide interlayers for improved cyclic stability of hybrid supercapacitors

Kyu Hyun Oh [‡], *Girish Sambhaji Gund* [‡], *Ho Seok Park**

[a]School of Chemical Engineering, Sungkyunkwan University (SKKU), 2066 Seobu-ro, Jangan-gu, Suwon-si, Gyeonggi-do, 440-746, South Korea.

[‡]*Kyu Hyun Oh* and *Girish Sambhaji Gund* contributed equally to this work.

***Corresponding author: Prof. Ho Seok Park (phs0727@skku.edu)**

Supplementary note 1: Analysis of $NiCo_2O_4$ nanoneedle growth

We have employed a hydrothermal method for the synthesis of $NiCo_2O_4$ nanoneedles. The orientation of nanostructure can be determined through several factors such as hydrodynamic forces, surface energy, surface roughness, etc. In the present work, hydrodynamic forces are similar owing to identical chemicals used and reaction parameters during a synthetic process. So, the nucleation and growth of the nanoneedle is driven by a minimization in free energy of the system based on surface energy between substrates and solution. The change in the Gibbs free energy of ΔG associated with the homogeneous nucleation process under the thermodynamic constraints of temperature and pressure is considered as follows [1-5]:

$$\Delta G_{homo} = \Delta G_s + \Delta G_v \quad \ldots\ldots(1)$$

where ΔG_s and ΔG_v are the Gibbs free energies required to create the crystal surface and to build the crystal volume, respectively. The change in the Gibbs free energy as a function of nucleation radius (r) can be expressed as below.

$$\Delta G_{homo} = 4\pi r^2 \Upsilon + \frac{4}{3}\pi r^3 \Delta G_v \quad \ldots\ldots(2)$$

where Υ is the interfacial energy.

The Gibbs free energy is minimized at equilibrium state, where critical radius (r_c) of the nucleation is achieved in chemical solution:

$$\frac{d\Delta G_{homo}}{dr} = 0 = 8\pi r_c \Upsilon + 4\pi r_c^2 \Delta G_v \quad \ldots\ldots(3)$$

Thus, the critical radius becomes:

$$r_c = -\frac{2\Upsilon}{\Delta G_v} \quad \ldots\ldots(4)$$

It notes that, ΔG_v is negative quantity and Υ is positive, so r_c will be positive quantity as expected. The equation (2) in terms of wetting angle for heterogeneous nucleation becomes:

$$\Delta G_{het} = \frac{(2 + cos\theta)(1 - cos\theta)^2}{4}\left(4\pi r^2 \Upsilon + \frac{4}{3}\pi r^3 \Delta G_v\right) \quad \ldots\ldots(5)$$

So, the critical radius size for heterogeneous nucleation becomes:

$$r_c^{het} = -\frac{2\Upsilon}{\Delta G_v} \quad \ldots\ldots(6)$$

Thus, the nucleation radius for heterogeneous growth on the substrate is directly proportional to interfacial surface energy (Υ).

The contact angle measurements demonstrated that the pristine nickel foam (NF) and rGO coated NF exhibited hydrophilic (contact angle = 0°) and hydrophobic (contact angle = 102°) nature of substrate, respectively. Since these values correspond to high and low surface energies, respectively, the low surface energy of rGO interlayers lead to restrict the growth of nanostructure towards the smaller dimension.

Supplementary note 2: XPS analysis

The high resolution XPS spectra of Ni 2p, Co 2p and C 1s of $NiCo_2O_4$@rGO hybrid and $NiCo_2O_4$ samples were shown in Fig. S4. The Ni $2P_{1/2}$, Ni $2P_{3/2}$, Co $2P_{1/2}$, and Co $P_{3/2}$ core level peaks of $NiCo_2O_4$@rGO hybrid were centered at 872.32, 855.15, 794.55, and 779.45 eV, respectively, and those of $NiCo_2O_4$ at 872.47, 855.31, 794.70, and 779.60 eV, respectively. The C1s core level of rGO could be fitted into three components assigned to C=C, C-O-C, and O-C=O peaks at 284.49, 285.08, and 288.70 eV. On the other hand, the C1s core level of $NiCo_2O_4$@rGO hybrid was deconvoluted into four components at 284.64, 284.50, 285.26, 286.29 and 288.29 eV, which are assigned to C=C, C-C, C-O-C, and O-C=O bonds, respectively. The negative peak shifts of Ni 2p and Co 2p, positive peak shift of C 1S for C=C bond, and peak broadening of O 1s for $NiCo_2O_4$@rGO hybrid confirmed interaction between $NiCo_2O_4$ and rGO. The specific interaction between $NiCo_2O_4$ and rGO was confirmed by the change in the oxidation state of Ni and Co in XPS spectra from the binding energies of Ni $2P_{1/2}$, Ni $2P_{3/2}$, Co $2P_{1/2}$, and Co $2P_{3/2}$, additional contribution in O 1s spectra though peak broadening, as well as in the sp^2-type hybridization of C from the binding energy of C 1S in XPS spectra.

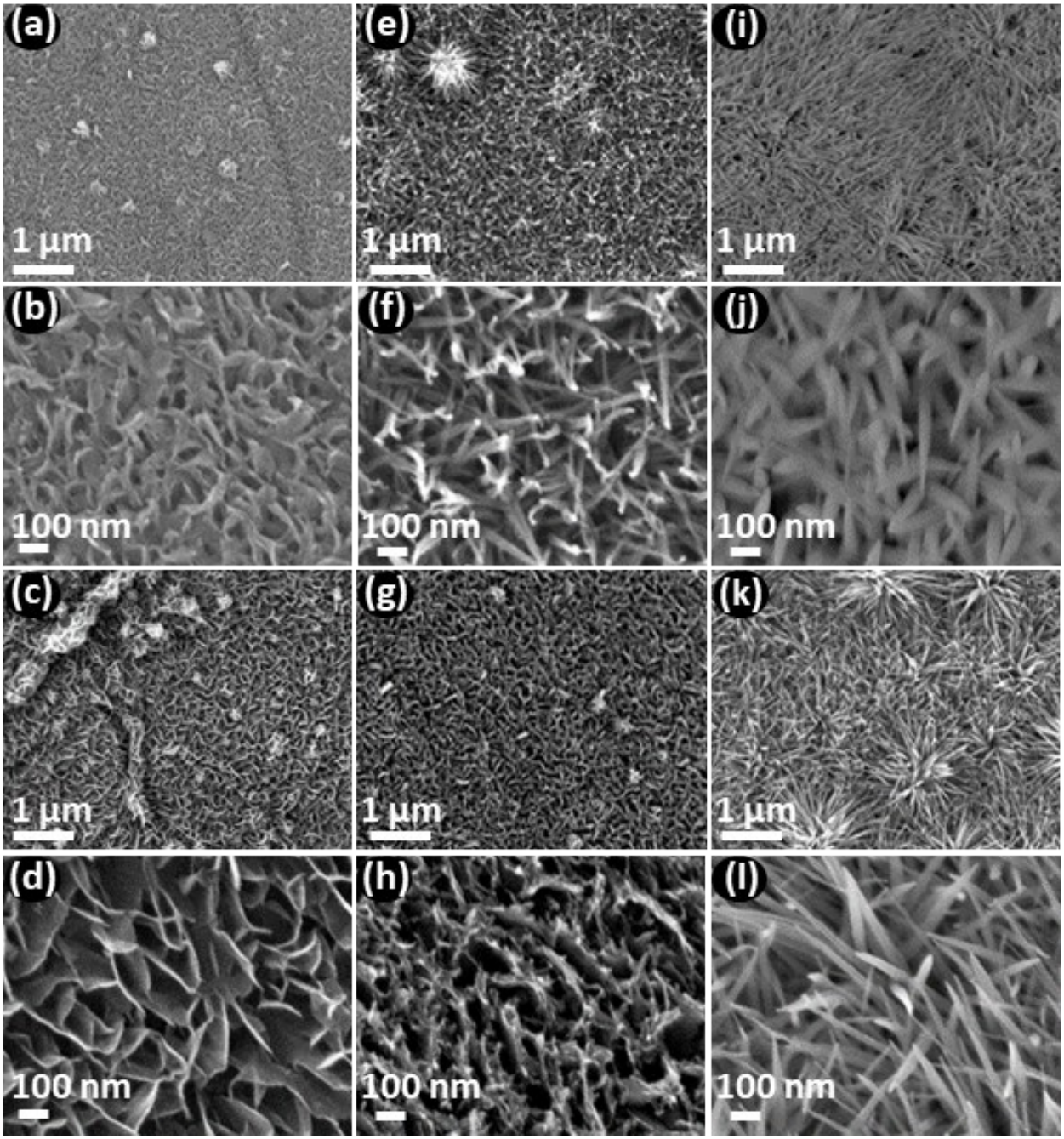

Figure. S1 FE_SEM images of $NiCo_2O_4$ nanostructures grown at different hydrothermal reaction times (a-d) 15 min, (e-h) 30 min, and (i-l) 1 hour on bare NF surface (a-b, e-f, i-j) and rGO coated on NF surface (c-d, g-h, k-l), respectively.

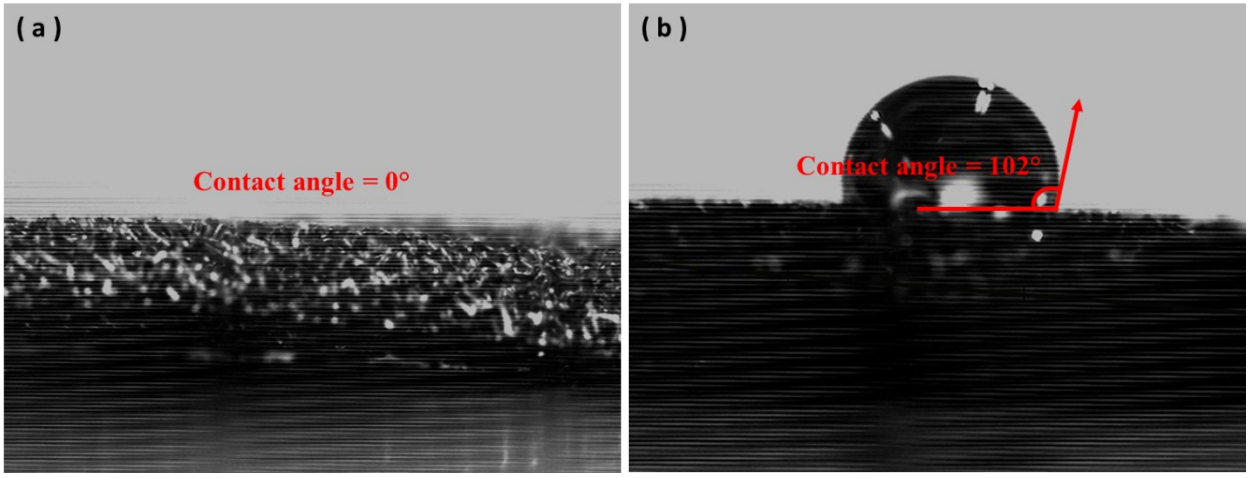

Figure. S2 Water contact angle images on (a) pristine NF and (b) rGO coated NF substrates.

$NiCo_2O_4$ (2θ)	Crystal size (nm)	Planes
31.1691	9.68	(220)
36.6726	10.37	(311)
44.5874	10.73	(400)
59.1270	9.66	(511)
64.9064	8.95	(440)

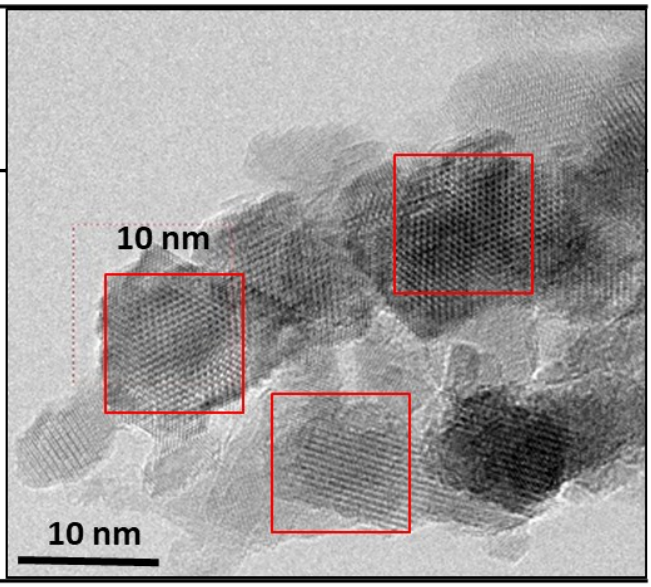

Figure. S3 Crystallographic features of $NiCo_2O_4$ nanoneedles from XRD and HR-TEM measurements.

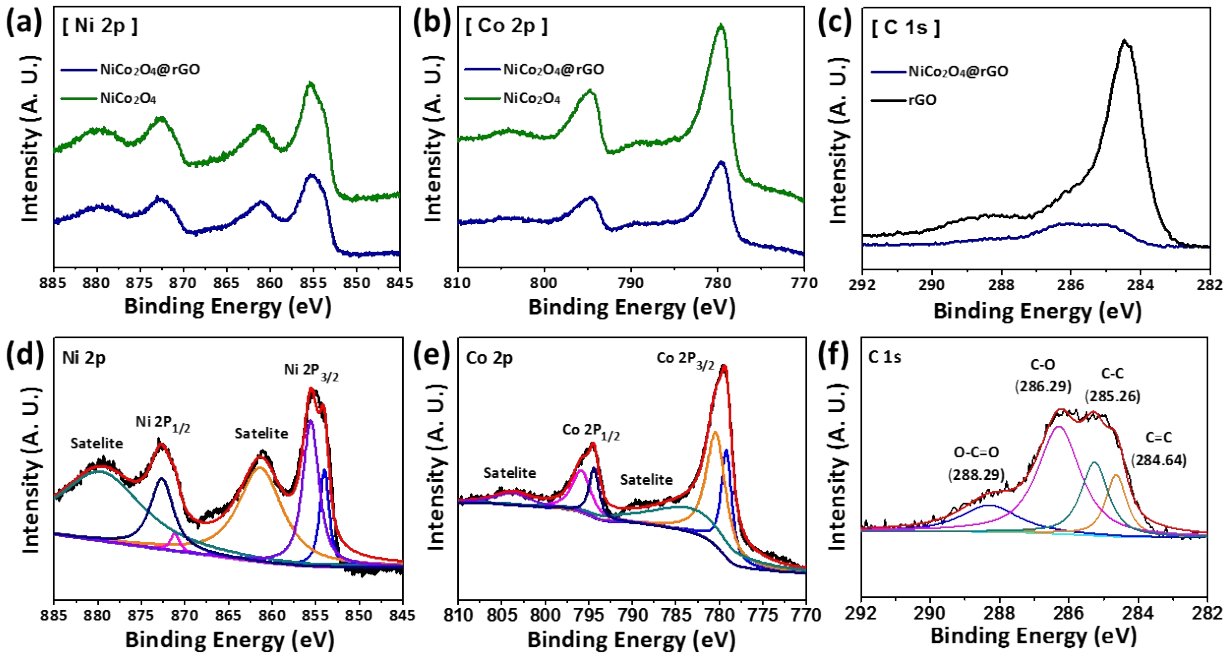

Figure. S4 High resolution XPS spectra of (a) Ni 2p and (b) Co 2p for $NiCo_2O_4$ and $NiCo_2O_4$@rGO hybrid, and (c) C 1s for rGO and $NiCo_2O_4$@rGO hybrid on NF. Deconvolution fitted XPS spectra of (d) Ni 2p and (e) Co 2p, and (f) C 1s for $NiCo_2O_4$@rGO hybrid on NF.

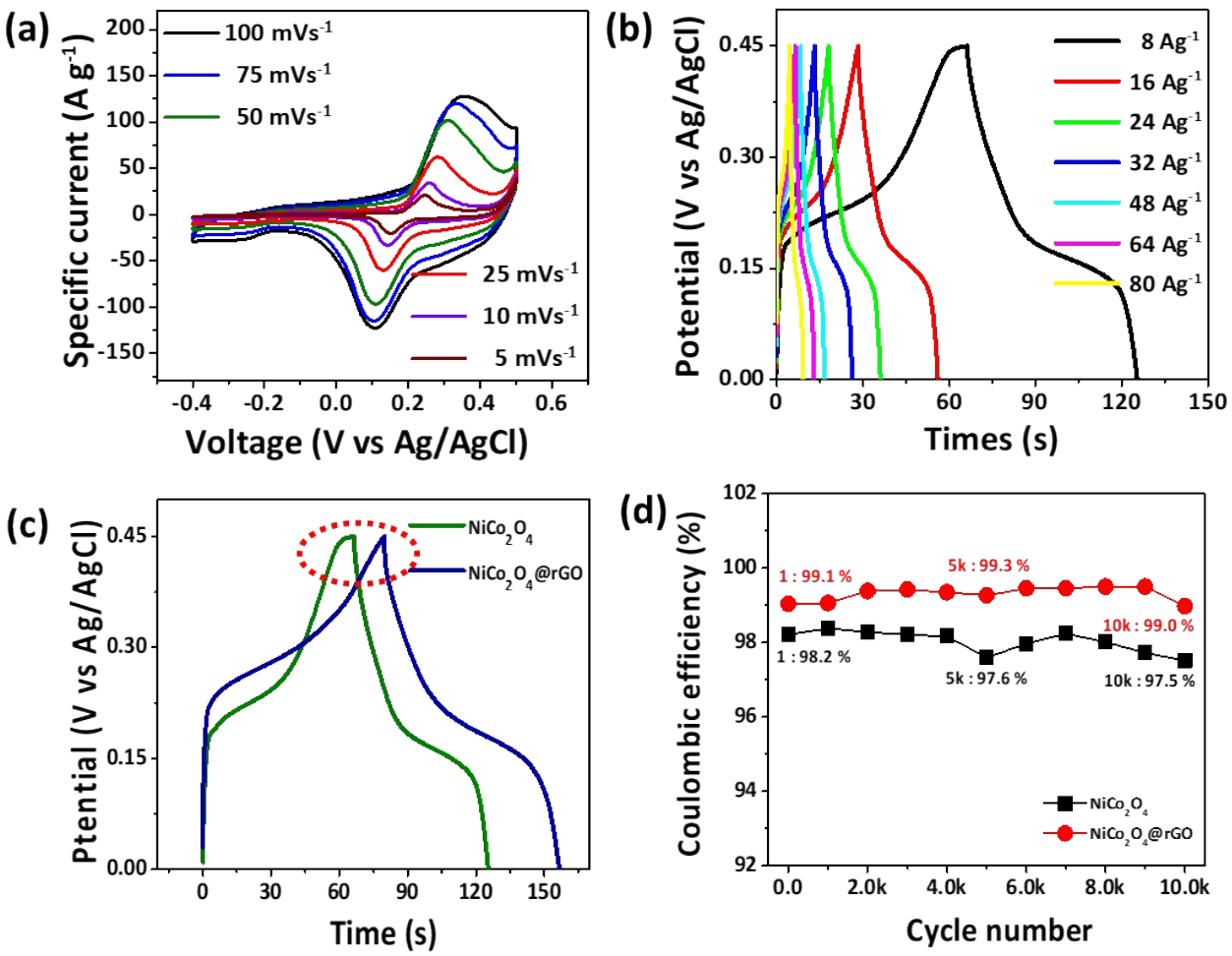

Figure. S5 (a) CV curves of $NiCo_2O_4$ electrode at different scan rate. (b) GCD profile of $NiCo_2O_4$ electrode at different current densities. (c) GCD curve of $NiCo_2O_4$ and $NiCo_2O_4$@rGO hybrid electrodes at constant current density of 8 A g^{-1}. (d) Coulombic efficiency variation of $NiCo_2O_4$ and $NiCo_2O_4$@rGO hybrid electrodes with GCD cycle number at 16 A g^{-1}.

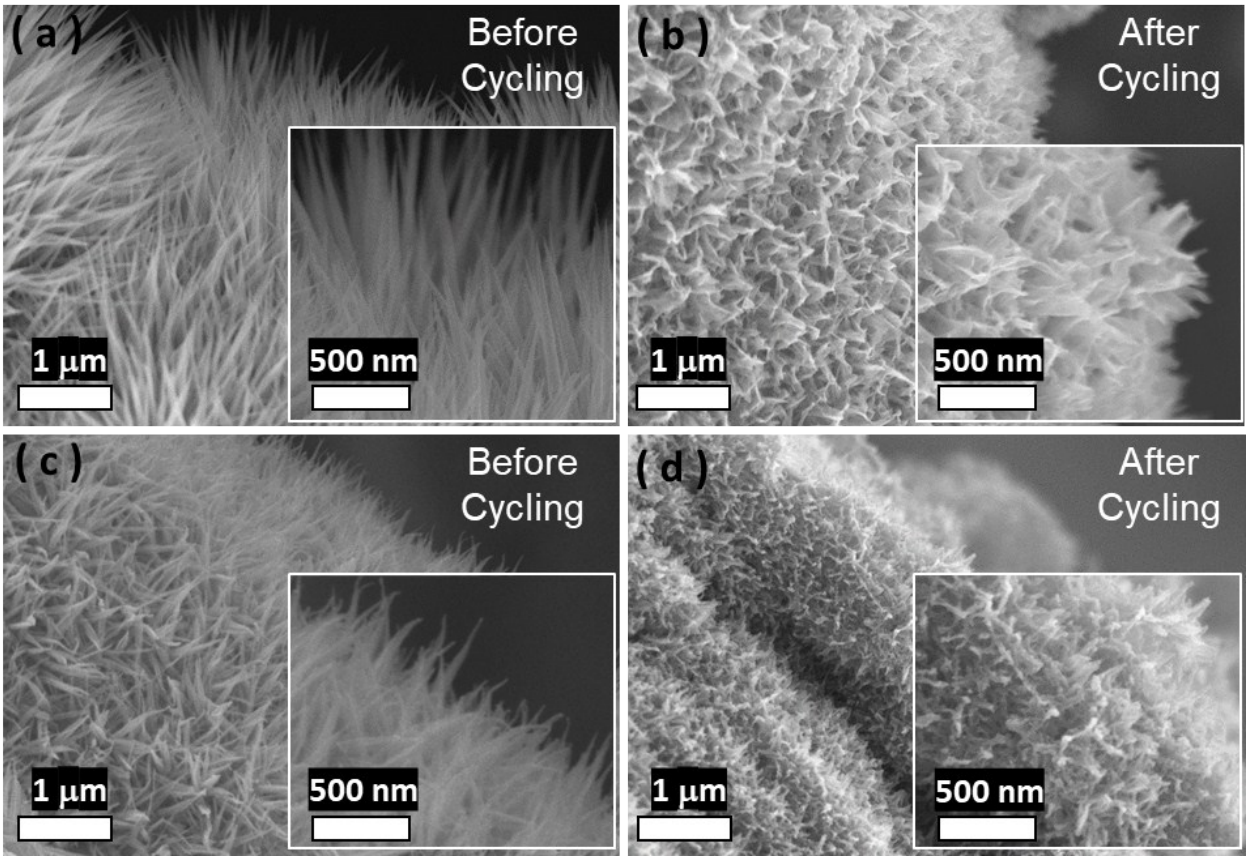

Figure. S6 FE-SEM images of $NiCo_2O_4$ and $NiCo_2O_4$@rGO hybrid electrodes before (a, c) and after (b, d) 10,000 GCD cycles at 16 A g^{-1}.

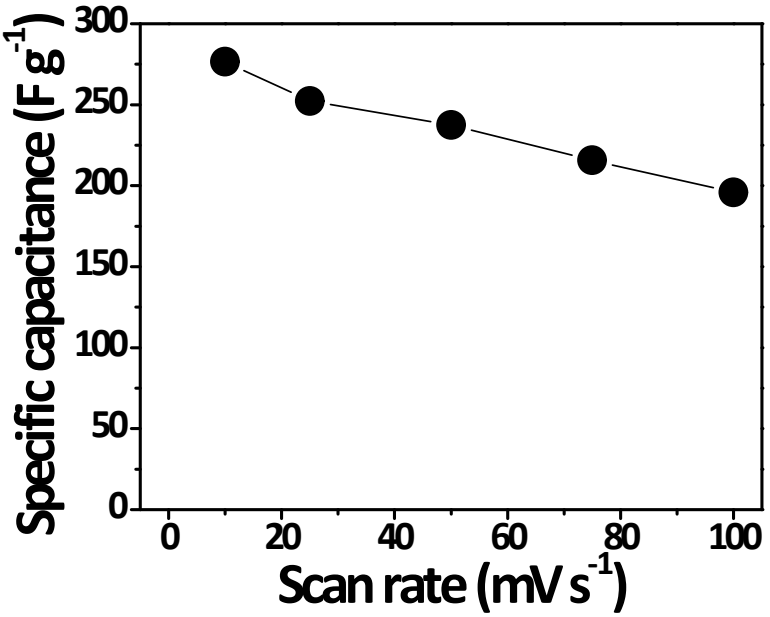

Figure. S7 Variation of specific capacitances of rGO electrode at different scan rates in 2 M KOH electrolyte.

References

[1] H. M. Kim, J. R. Youn, Y. S. Song, Prog. Mater. Sci., 2014, **64**, 121–199.

[2] C. J. O'Kelly, S. J. Jung, J. J. Boland, Cryst. Growth Des., 2016, **16**, 7318−7324.

[3] H. M. Kim, J. R. Youn, Y. S. Song, Nanotechnology, 2016, **27**, 085704.

[4] David A Porter, Kenneth E Easterling, Mohamed Y Sherif, Phase Transformations in Metals and Alloys Third Edition, CRC Press, 2009.

[5] V. Raghavan, Solid state phase transformations First edition, Prentice Hall of India Pvt. Ltd., 1992.